Simulation study of sulfonate cluster swelling in ionomers

Elshad Allahyarov
Department of Physics, Case Western Reserve University, Cleveland, Ohio 44106, USA; OIVTRAN, Joint Laboratory of Soft Matter, Moscow 127412, Russia; and Institut für Theoretische Physik II, HHU Düsseldorf, Universitätstrasse 1, 40225 Düsseldorf, Germany

Philip L. Taylor
Department of Physics, Case Western Reserve University, Cleveland, Ohio 44106, USA

Hartmut Löwen
Institut für Theoretische Physik II, HHU Düsseldorf, Universitätstrasse 1, 40225 Düsseldorf, Germany

(Received 2 September 2009; published 30 December 2009)

We have performed simulations to study how increasing humidity affects the structure of Nafion-like ionomers under conditions of low sulfonate concentration and low humidity. At the onset of membrane hydration, the clusters split into smaller parts. These subsequently swell, but then maintain constant the number of sulfonates per cluster. We find that the distribution of water in low-sulfonate membranes depends strongly on the sulfonate concentration. For a relatively low sulfonate concentration, nearly all the side-chain terminal groups are within cluster formations, and the average water loading per cluster matches the water content of membrane. However, for a relatively higher sulfonate concentration the water-to-sulfonate ratio becomes nonuniform. The clusters become wetter, while the intercluster bridges become drier. We note the formation of unusual shells of water-rich material that surround the sulfonate clusters.

DOI: 10.1103/PhysRevE.80.061802 PACS number(s): 61.41.+e, 82.47.Nj, 64.75.St, 82.47.Gh

I. INTRODUCTION

An interest in ionomers, i.e., ion-containing polymers, began 50 years ago with the development of organic ion-exchange resins [1]. The properties of these materials are completely different from those of other polymers as a consequence of the ionization of the ionic groups in polar solvents. The specificity of the interaction between the ion, the solvent, and the polymer makes it possible for these materials to be used as perm-selective membranes, thermoplastics or films for microencapsulation and coating [2]. A significant interest in ionomer materials also stems from their growing application as a polymer electrolyte membrane (PEM) or a proton exchange membrane in fuel cell technology [3–6].

DuPont de Nemours was the first manufacturer in the early 1960s to develop a perfluorosulfonic membrane commercially [7,8]. This membrane, which was named Nafion®, consists of a polytetrafluoroethylene hydrophobic backbone to which perfluorovinyl ether pendant side chains are attached at more or less equally spaced intervals. The pendant chains are terminated by sulfonic head groups SO_3H, and these are responsible for the large variety of microstructures in which the ionomer can be assembled. When exposed to humidity, the membrane takes up large amounts of water, leading to the dissociation of the acid groups $SO_3H \rightarrow SO_3^- + H^+$ and to the formation of a nanophase-separated network of aqueous (hydrophilic) clusters and hydrophobic polymer. According to the cluster morphology model of Hsu and Gierke [9], spherical clusters are uniformly distributed throughout the material and are interconnected by channels [10,11]. Subsequent cluster-based models, such as the Mauritz-Hopfinger model [12,13], the Yeager three-phase model [14], the Eisenberg model of clusters of hydrocarbon ionomers [15], and the Litt model of a lamellar morphology for sulfonate domains [16], have tried to quantify the cluster radius and spacing as a function of the polymer equivalent weight and the hydration level. Other structural models were proposed to describe the membrane swelling process from a dry state to a colloidal suspension as a continuous process [17,18].

There is still ongoing debate about which one of the proposed models is more suitable and effective in representing the ionomer's conductivity through its nanophase separated network of hydrophilic regions. The issue is complicated by the fact that experimental studies show the ionomer structure to depend on the pretreatment methods used in its preparation [8,19–23]. The membrane pretreatment serves to reduce the remnant anisotropy in the morphology of extruded membranes, and to clean a solvent-cast membrane from impurities [13,24]. Rigorously speaking, the question of how the pretreatment steps, such as swelling and/or boiling in solvents, annealing, rinsing in water, drying in vacuum/air, and the order of these steps, affect the membrane morphology, is not yet answered. Most of the pretreatment protocols have the ultimate goal of improving the water uptake of the membrane [20,25]. For example, in Ref. [20] it has been shown that the water uptake of a dry membrane depends on how it was dried from its swollen state at elevated temperatures. If it was first cooled and then dried, then the membrane keeps its swollen volume. But if it was first dried and then cooled, the membrane shrinks in volume during the drying process. As a result, the outcome of the first protocol is a membrane that takes up a desirably large amount of water, and thus has a better ion conductivity.

The water solvation of a PEM, which is necessary for its efficient operation, reduces its working temperature range: the membrane will not be exploitable at freezing and boiling water temperatures. A possible way to overcome this limitation is the development of new membranes that can operate at the low wetting conditions where λ, which is the number

of water molecules per sulfonate group, is less than five. In the case of full hydration there are five water molecules in the primary hydration shell of a sulfonate [26–28]. In low-humidity membranes, the protons diffuse along narrow pathways near the SO_3^- terminals of side chains, and two conflicting effects come into play. On the one hand, the proximity of negatively charged sulfonates considerably suppresses the mobility of the protons. On the other hand, when the separation distance between sulfonates is small, the activation energy for proton hopping between adjacent end-groups becomes comparable with the activation energy in the bulk water [29], making the net result unclear. The proton mobility in low-humidity membranes can be also elevated by adding flexibility to the side chains, and by modifying the network structure of side-chain clusters.

Despite the fact that various models have emerged to explain the properties of hydrated Nafion membranes, a systematic study of how the molar concentration η of sulfonate head groups and the solvent content parameter λ affect the network structure of sulfonates, and particularly the swelling of single clusters has not yet appeared. This absence is important for understanding ion transport and the onset of percolation in low-humidity membranes, and forms the motivation for this study.

Here we perform simulations to investigate the dependence of the cluster swelling on the hydration level λ and the sulfonate molar concentration η of the membrane by employing different side-chain architecture models. We restrict ourselves to the case of ionomers for which there is no bulk water inside the sulfonate clusters, and in which the sulfonate concentration is considerably below the percolation limit for the head groups. It is expected that in these *low-humidity* and *low-sulfonate* membranes no overlapping between sulfonate clusters takes place. In order to distinguish a sulfonate cluster from a water cluster, which is necessary in the interpretation of our simulation results, for the former we adopt the term "sulfonate multiplet," first introduced by Eisenberg in Ref. [15] to describe the primary aggregates of sulfonates. We show that at the onset of swelling, which is defined as the transition from a dry multiplet into a wet multiplet with dissociated ions, the multiplets split into smaller parts. The solvation of these resultant multiplets is analyzed for different hydration levels and sulfonate concentrations. In particular, we will demonstrate the formation of water shells around the sulfonate multiplets.

The paper is organized as follows. In Sec. II we briefly discuss the benefits of using coarse-grained models (as opposed to all-atomistic approaches), and describe the coarse-grained model and system parameters employed here. The simulation details are outlined in Sec. III. Results on multiplet formation in dry and solvated membranes, water shells around multiplets, ionomer deformation, and ion diffusion are discussed in Sec. IV. We conclude in Sec. V.

II. COARSE-GRAINED SYSTEM PARAMETERS

Despite the rich variety of experimental findings and theoretical predictions for the ordered morphology in PEM materials, numerical experiments have so far had little success in finding any clear picture of cluster formation in hydrated membranes. The main reason for this is the fact that individual ionic clusters are about 2–5 nm in size, and this is usually comparable to, or even larger than, the system sizes affordable in all-atomistic modeling. As a result, atomistic simulations, which are quite helpful for understanding the simple pore physics and small ionomer molecular conformations, are not able to capture the distribution of sulfonate clusters in the hydrophobic matrix. However, as already outlined in the Introduction, knowledge of this distribution is crucial for the determination of the ionomer connectivity and the ion conductivity of the PEM material.

Fortunately polymers show a large degree of universality in their static and dynamic behavior. The universal scaling properties of the ionomer as a function of chain length, sulfonate density, and membrane composition can be most efficiently studied via coarse-grained molecular models. One of the most commonly employed systems is a bead-spring model, where each bead represents a segment of a realistic chain. Wescott *et al.* [30] and Wu *et al.* [31] have simulated large ionomer systems using coarse-grained approaches in which an entire side chain was represented by a nanometer-size hydrophilic blob. Their simulations report irregularly shaped hydrophilic clusters embedded into the polymeric matrix of backbone chains. While such gross coarse graining is computationally convenient, it is not possible to draw firm conclusions regarding ion diffusion from the conformational results obtained for the polymer. It is therefore necessary to limit the coarse-graining approach to the level at which the sulfonic acid groups of the polymer can be explicitly treated, as these groups contain the essential membrane-specific interaction sites relevant to absorbed water and conducting ions.

In our 'united atom' approximation for Nafion, the ether oxygens and sulfur atoms are treated individually, while the fluorocarbon groups are consolidated as a single particle, as are the three oxygens of the sulfonate [32–34]. The fluorocarbon groups, the sulfonate oxygens, the sulfur atoms, and the ions are modeled as single Lennard-Jones (LJ) particles with a diameter $\sigma=0.35$ nm. The ions carry the full formal charge of $Q_p=+e$, the sulfur atoms have $Q_S=+1.1e$, and the combined triplet of oxygen atoms carries $Q_{O_3}=-2.1e$. The partial charges of the ether oxygens and the fluorocarbon LJ particles are set to zero. Depending on whether the membrane is dry or hydrated, two different representations have been used for the sulfonate head groups. For dry membranes, we implement an attached-ion model, also called a dipole model for head groups, which was extensively analyzed in our previous paper [32]. Though the attached-ion model does not allow for ion diffusion, it is considered as a good starting point for a step-by-step exploration of nanophase morphology in PEM materials. For the hydrated ionomer we assume a detached-ion model [33,35], where the ions diffuse freely in the system, where they interact with ionized head groups and water molecules.

The configurational part of the coarse-grained Hamiltonian for the attached and detached ion models is a combination of Coulomb interactions, nonbonded, and bonded interactions between all the ionomer components,

$$U_{\text{total}} = U_{LJ} + U_Q + U_{\text{bond}} + U_{\text{angle}} + U_{\text{dihedral}}. \quad (1)$$

Here U_{total}, U_{LJ}, U_Q, U_{bond}, U_{angle}, and U_{dihedral} are the total potential energy and its Lennard-Jones, electrostatic, bond-stretching (bond-length term), angle bending (bond-angle term), and dihedral angle components, respectively,

$$U_{LJ}(r) = 4\varepsilon_{LJ}\sum_{i>j}[(\sigma/r_{ij})^{12} - a(\sigma/r_{ij})^{6}], \quad (2)$$

$$U_Q = \sum_{i>j}\frac{Q_iQ_j}{\epsilon rij}, \quad (3)$$

$$U_{\text{bond}}(r) = \frac{1}{2}\sum_{\text{all bonds}} k_b(r - r_0)^2, \quad (4)$$

$$U_{\text{angle}}(\theta) = \frac{1}{2}\sum_{\text{all angles}} k_\theta(\theta - \theta_0)^2, \quad (5)$$

$$U_{\text{dihedral}}(\alpha) = \frac{1}{2}\sum_{\text{all dihedrals}} k_\alpha(1 - d\cos(3\alpha)). \quad (6)$$

In Eq. (2) the LJ interaction coefficient ε_{LJ} in units of k_BT was chosen to be 0.33. The parameter a in the LJ term is 1 for hydrophobic-hydrophobic (HH) interactions, and 0.5 for hydrophobic-hydrophilic (HP) interactions and hydrophilic-hydrophilic (PP) interactions. In the latter case only the repulsive part of the LJ potential (a shifted LJ potential for $r < 1.1224\sigma$) has been considered. In Eq. (3), Q_i and Q_j are the electrostatic charges of the two interacting elements, which can be sulfur atoms, oxygen triplets, ions, or the hydrogens or oxygen of the water molecules, and ϵ is the dielectric constant of the ionomer. In Eqs. (4)–(6) the following force-field parameters have been used: the equilibrium bending angle $\theta_0 = 110°$, the equilibrium bond length $r_0 = 0.44\sigma$, the bending force constant $k_\theta = 120\frac{\text{kcal}}{\text{mol deg}^2}$ and the stretching force constant $k_b = 7\times10^4\frac{\text{kcal}}{\text{mol(nm)}^2}$. The dihedral angle parameters were $d = -1(+1)$ and $k_\alpha = 10.8k_BT$ ($k_\alpha = 3.7k_BT$) for the backbone (side chain) segments.

The dielectric properties of the coarse-grained material are represented by a distance-dependent dielectric function,

$$\epsilon(r) = 1 + \epsilon_B(1 - r/\sigma)^{10}/[1 + (r/\sigma)^{10}], \quad (7)$$

where ϵ_B is the bulk dielectric constants of the ionomer. Usually a uniform permittivity $\epsilon = 1$, or equivalently $\epsilon_B = 0$ in Eq. (7), is accepted in *ab initio* quantum-mechanical simulations, where all the ionomer atoms are explicitly taken into account. Since the coarse-grained approach neglects the atomistic structure of the ionomer monomers, additional approximations for the dielectric permittivity have to be made to account for the polarization effects of the ionomer monomers as a response to the strong electrostatic fields of the sulfonate groups and ions. To be accurate, $\epsilon(r)$ should depend upon the atom types and the absolute values of all the explicit coordinates. The problem, of course, is that the specific form of $\epsilon(r)$ is not known. Hence the distance-dependent dielectric permittivity is a free parameter of our model. It seems quite natural to suggest that the polarization permittivity should increase with distance, and approach a bulk value between 4 and 8, which corresponds to the bulk permittivity of dry Nafion as measured in high-frequency studies [19] and differential scanning calorimetry [36], and from first-principle calculations [37]. Our choice for the distance-dependent permittivity given by Eq. (7) qualitatively follows the trend of dielectric saturation effects: it smoothly increases from 1 at touching separations, when there is no polymer material between two charges, towards 6, when two charges are at the maximal separation $L/\sqrt{2}$ allowed in a periodically repeated box of size L. The polarization-related saturation effects, according to Eq. (7), appear at distances larger than 100 nm, which are beyond the typical separations in a simulated system.

TABLE I. Parameters used in simulation runs. Here n_1+n_2 is the total number of monomers per side chain, λ is the water content per head group.

Runs	Hydration model	n_1+n_2
Run 1	Dry ionomer with no water, λ=0	10
Run 2	Ionomer with explicit water, λ=1	9
Run 3	Ionomer with explicit water, λ=3	9
Run 4	Ionomer with explicit water, λ=5	9

Taking into account the fact that the sulfonic acid tips of side chains are hydrophilic, and the remaining part of side chains, as well as the backbone polymer, are hydrophobic [38,39], we use the following notation to describe the polymer architecture: n_1H+n_2P for side chains and n_3H for the backbone segments. Here n_1 is the number of hydrophobic monomers per side chain, n_2 is the number of hydrophilic monomers per side chain, and n_3 is the number of backbone monomers between two adjacent side chains. The total number of side-chain monomers per pendant chain is n_1+n_2 in the detached ion model, and n_1+n_2+1 in the attached-ion model.

III. SIMULATION DETAILS

Extensive coarse-grained molecular dynamics (MD) simulations were performed to investigate the swelling properties of sulfonate multiplets at four different solvation parameters λ and two distinct sulfonate molar concentrations η. The parameter η is defined as $\eta \equiv (N_S/N_0)V$, where N_S is the number of side chains in the volume $V = L^3$ of the simulation cell, and N_0 is Avogadro's number. Whereas in experimental studies the parameters η and λ are coupled to each other [40], in numerical simulations both quantities can be changed independently. A series of simulation runs are summarized in Table I. The molar concentrations $\eta_1 = 0.8$ mol/l and $\eta_2 = 1.5$ mol/l correspond to the backbone segment lengths $n_3 = 50$ and $n_3 = 20$, respectively. Varying the parameter η, i.e., varying the chain volume per SO_3^- group, is in some ways equivalent to simulating materials with different equivalent weights [40]. For convenience, we will refer to the membrane with sulfonic molar concentration η as "membrane η." In most simulations of Nafion-like ionomers

the parameter n_3 is usually varied between 14 and 18. Shorter segments with $n_3=10$ have been considered in the atomistic simulations of Ref. [41], and longer segments $n_3=30$ in the coarse-grained approaches of Ref. [60]. In the latter case the nearest-neighbor distance between the sulfonate multiplets is large. Thus our choice of a larger n_3 makes possible the investigation of the solvation properties of single multiplets in slightly hydrated membranes.

There were $N=(n_1+n_2+n_3)\times N_S$ polymer monomers in the simulation box of length L. All simulations were carried out for both the $n_1=7$ and $n_2=2$ side-chain architectures. The number of side chains N_S was 500 for membrane η_1 and 1000 for membrane η_2. The negative charges of N_S sulfonate groups were compensated by N_S positive ions to guarantee an overall charge neutrality in the system. The charge and size of the model ion affect its diffusion through the membrane, since they define the ion binding to sulfonates which affects the ion mobility. In elaborate proton models [42–44] the proton charge is varied between $+0.4e$ and $+0.6e$ and the protons are considered tightly associated with water oxygens and water molecules. These models invoke different coarse-grained parameters, such as partial charges and monomer sizes for the ether oxygens, sulfur atoms, and the fluorocarbon groups. Our ion can be considered as a larger hydronium complex of charge $+e$, an approach based on the fact that a proton detached from a sulfonate instantly captures a water molecule and becomes a hydronium ion [27]. Simulations with explicit water include an additional $3\times\lambda\times N_S$ water charges, as we are using three-point TIP3P solvent model [44,45]. The box size L was systematically increased from $L=10.5$ nm to $L=11.4$ nm when the water content λ was increased from $\lambda=0$ to $\lambda=5$ in order to keep the density of the hydrated membrane constant.

One of the main challenges in generic ionomer simulations is the fact that the ionomer molecule is quite stiff at ambient temperatures and low humidity conditions. In experimental studies a fast ionomer equilibration is usually achieved through different pretreatments protocols, such as a soaking in a solvent or high-temperature annealing. These steps improve the side-chain kinetics and decrease the barrier between the trapped metastable states and the low-lying states at the global minimum in free energy. Overall, a full equilibration, even after these pretreatment steps, takes hours or days, a time span that is far beyond the feasible simulation times of several nanoseconds in typical molecular dynamics runs. To overcome this obstacle we implemented the following artificial steps [46]:

(a) the side chains were temporarily detached from the backbone skeleton, a technique that has been successfully applied in Refs. [33,35,43,47,48],

(b) the skeleton was cut into smaller segments of length n_3.

The resulting "fragmented" ionomer reaches the equilibrium state very fast because of the increased diffusive movement of its segments. Typical MD runs of 500 ps duration in the *NVT* ensemble were enough to fully equilibrate the simulated system. The system temperature T was controlled by coupling the ionomer to a Langevin thermostat with a friction coefficient $\gamma=10$ ps^{-1} and a Gaussian white-noise force of strength $6k_BT\gamma$. The equations of motion were integrated using the velocity Verlet algorithm with a time step of 0.25 fs. We also imposed standard periodic boundary conditions to our system, thus filling space with translational replications of a fundamental cell. Long-range electrostatic interactions were treated using the Lekner summation algorithm [49].

In the next stage of the simulations, the ionomer segments were reassembled back into a branched chain characterizing the original Nafion-like ionomer. This was achieved by a simultaneous introduction of bonds and angular constraints between the ends of backbone segments unifying them into a single and long backbone chain. Similar bond and angular constraints were introduced between the fluorocarbon tail monomers of detached side chains and the median section monomers of backbone segments. To avoid the formation of unphysical starlike branches only a single occupancy of backbone attachment sites was permitted. The simulations were then resumed for another few hundred picoseconds until a new equilibrium state was reached. Then the statistically averaged quantities of interest were gathered during the next 3–5 ns of the long production runs.

The question arises as to whether this artificial membrane treatment produces a truly equilibrated state. We ran test simulations for solvated membrane with $\lambda=5$ in which we did not adopt the procedure of detaching and segmenting the side chains and backbones and then reattaching them, but instead left them intact. After a very long time the system did reach a point where the results were equivalent to those achieved much more rapidly in the earlier procedure. However, for a completely dry system even long simulations of several nanoseconds duration were not sufficient to achieve a completely equilibrated system. It is similarly difficult to mimic existing experimental procedures for membrane equilibration, such as casting the membrane from dilute solution, or gradual quenching of high-temperature ionomers down to room temperature. We do acknowledge that the procedures implemented in this work for quick equilibration of a randomly generated ionomer might bias the head-group cluster formation, but note that once the membrane was fully equilibrated, no morphological changes were detected during the production runs or during additional runs with start-up configurations taken from the final structures of previous 2–3 ns runs.

IV. SIMULATION RESULTS

A. Multiplet formations in dry and solvated membranes

A typical snapshot of a hydrated membrane from Run 3 is shown in Fig. 1. The backbone skeleton, plotted as lines, creates a hydrophobic network with chaotically scattered pores. These pores incorporate micellelike clusters of side-chain sulfonates (shown as spheres), which are filled with water molecules and ions. The number densities $\rho(\vec{r})$ of the hydrophobic part of the ionomer and of the absorbed water, averaged over a 100 fs run (following a lengthy equilibration), are shown in Figs. 2 and 3, respectively. The density $\rho(\vec{r})$ corresponds to the probability of finding a particular membrane component, hydrophobic monomer or hydrophilic water, at the point $\vec{r}$ during a short simulation run. The qua-

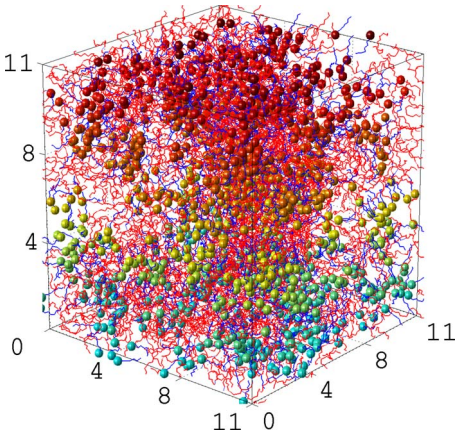

FIG. 1. (Color online) A typical snapshot of hydrated membrane η_2 from Run 3. The spheres represent the end-group oxygens of the side chains. The polymer is shown by red lines. Different bead colors correspond to different bead altitudes, with a blue color (gray in printed version) for low-altitude beads (at the bottom of simulation box) and a red color (black in printed version) for high-altitude beads (at the top of simulation box). The size of all structural elements is schematic rather than space filling. The water molecules and ions are not shown for the sake of clarity. The axis dimension is in nm.

siregular network of polymer skeleton with interconnected hydrophilic pores changes its form slowly with time.

The structure of the sulfonate multiplets was probed through the calculation of the sulfonate-sulfonate pair correlation function,

$$g_{SS}(r) = \frac{V}{N_S} \frac{dn_S(r)}{4\pi r^2 dr}. \tag{8}$$

Here $dn_S(r)$ is the number of sulfurs located at the distance r in a shell of a thickness dr from a fixed sulfur atom. The function $g_{SS}(r)$ indicates the probability of finding two sulfonate monomers at a separation distance r averaged over the equilibrium trajectory of the simulated system. Simulation results for $g_{SS}(r)$ for Runs 1–4 from Table I are shown in Fig. 4. The dry multiplets have no detectable internal structure except the strong maximum at $r \approx 0.5$ nm. In hydrated membranes the correlation function g_{SS} shows shell-like oscillations, a recognizable fingerprint of solvation shells. The first maximum of $g_{SS}(r)$ corresponds to the closest-approach configuration between neighboring sulfonates. The second peak of $g_{SS}(r)$ stems from a configuration where two neighboring sulfonates are separated by single ion or water molecule. Finally, the third peak of $g_{SS}(r)$ is related to configurations with more than one ion or water molecule between sulfonates. The dependence of the intensity of the correlations between the head groups on water content λ is due to the dielectric screening properties of water: the more the water content in the membrane, the weaker the sulfonate-sulfonate interactions. Similar results have been reported in the simulation results of Refs. [50–53]. The greatly reduced intensity of the first peak of $g_{SS}(r)$ at $\lambda = 5$ can be understood as the onset of the improbability of the closest-approach sulfonate-sulfonate configurations in hydrated multiplets.

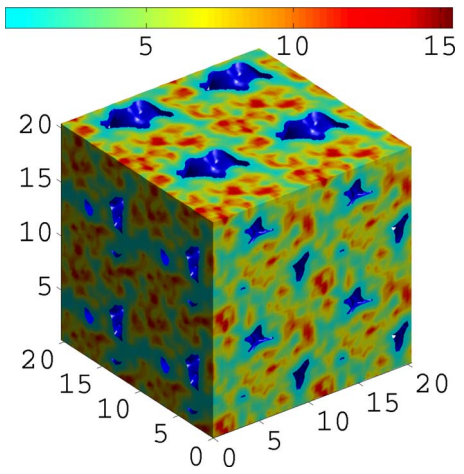

FIG. 2. (Color online) Three-dimensional (3D) density $\rho(\vec{r})$ of the hydrophobic part of the membrane η_2 for Run 3. The color gradient from blue (gray in printed version) to red (black in printed version), corresponds to the variation of membrane density from low to high values. The axis dimension is in nm.

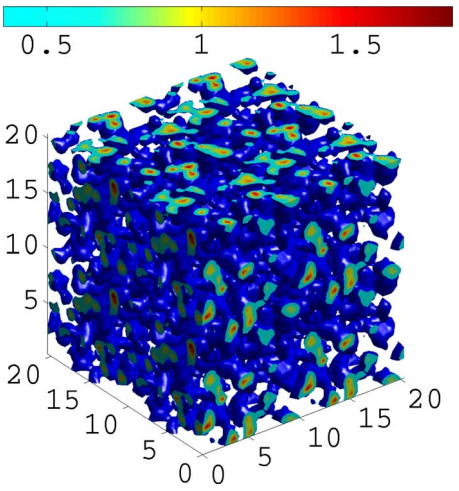

FIG. 3. (Color online) 3D density of water channels for the membrane η_2 and Run 3. The color gradient from blue (gray in printed version) to red (black in printed version) corresponds to the variation of water density from low values to high values. The axis dimension is in nm.

We determine the size of a multiplet as the position of the global minimum R_A^S (also known as the radius of the first coordination sphere) of the pair correlation functions g_{SS} in Fig. 4. This position depends on the membrane hydration level λ, and can be used to calculate the number of head groups χ_S inside the multiplet according to the following relation:

$$\chi_S = \frac{N_S}{V} \int_0^{R_A^S} g_{SS}(r) 4\pi r^2 dr. \tag{9}$$

The calculated values for the parameters R_A^S and χ_S are given in Table II for the membranes η_1 and η_2. There is a clear indication of the fact that the multiplets shrink in size at the onset of membrane solvation, which corresponds to the tran-

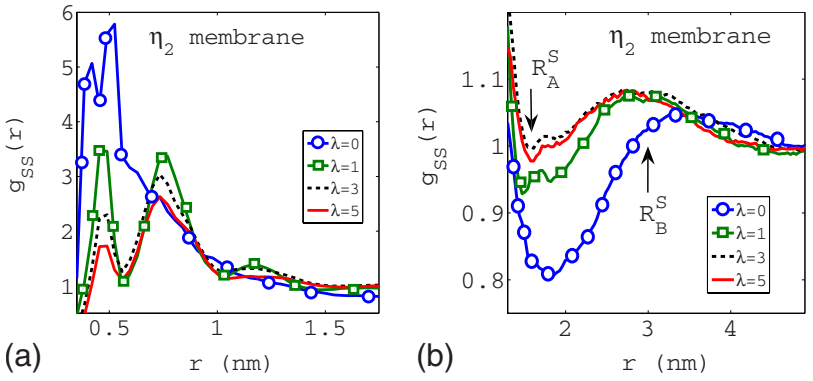

FIG. 4. (Color online) Sulfonate-sulfonate pair correlation function $g_{SS}(r)$ for membrane η_2 as a function of sulfur-sulfur separation distance r for Runs 1–4 from Table I. Solid blue line with circles—Run 1, solid green lines with squares-Run 2, dashed black line-Run 3, full red line-Run 4. The bottom figure shows in detail the long-range tail of $g_{SS}(r)$ used to determine the average multiplet size R_A^S and the separation distance between the sulfonate multiplets R_B^S. The calculated values for the parameters R_A^S and R_B^S are given in Table II.

sition from Run 1 to Run 2. This shrinking, which is not in accord with the classical theories of cluster swelling in ionomers, is accompanied by a multiplet splitting into smaller parts. For instance, the dry multiplet in the membrane η_2 has a size $R_A^S=1.75$ nm and consists of $\chi_S=22$ head groups. Following hydration by a water content as low as $\lambda=1$, this multiplet effectively splits into two smaller parts of size $R_A^S=1.47$ nm, each of them consisting of only 13 head groups. These small multiplets will consequently swell, keeping the number of their sulfonate population constant, when additional water is absorbed into the membrane. The swelling radius is largely determined by the competition between two different internal energies, the elastic energy of the backbone material and the electrostatic energy of the pendant groups.

The pair correlation functions $g_{SS}(r)$ for two different sulfonate concentrations η_1 and η_2 are plotted in Fig. 5. When the parameter η decreases, (as seen by a comparison of the thin and thick lines in Fig. 5), the intensity of sulfur-sulfur correlations increases. This effect stems from the interplay between the electrostatic screening length l_D and the average separation distance $\bar{l}$ between the sulfonates. For an ionomer with a high sulfonate concentration η, one generally has $l_D<\bar{l}$, and thus the electrostatic correlations between the sulfonates are negligible. In this case a nanophase separation in the membrane is possible only due to the hydrophobic/hydrophilic immiscibility between the backbone and side-chain segments of the membrane. In the opposite case, when η is small and $l_D>\bar{l}$, the Coulomb correlations become sufficiently strong to force the sulfonates to form compact multiplets.

B. Separation distance between multiplets

It is a well established fact that the nearest-neighbor separation distance between the multiplets and the connectivity of multiplets into a network of hydrophilic pathways are the main contributing factors to the transport properties of ionomers. The typical multiplet-multiplet nearest-neighbor distances can be directly deduced from the density-density correlations in the network of head groups by consideration of the structure factor,

$$S(\vec{q}) = N_S^{-1}\left\langle \left[\sum_{i=1}^{N_S}\cos(\vec{q}\cdot\vec{r}_i)\right]^2 + \left[\sum_{i=1}^{N_S}\sin(\vec{q}\cdot\vec{r}_i)\right]^2 \right\rangle. \tag{10}$$

When there is no preferential ordering of the hydrophilic domains in the membrane, the structure factor of the sul-

TABLE II. Calculated ionomer parameters for membranes with sulfonic molar concentration η_1 and η_2 (abbreviated as membranes η_1 and η_2 in the text). The parameters R_A^S, R_A^W are the size of sulfonate-sulfonate multiplets and water clusters, respectively, and are given in nm. The parameters R_B^S and R_B^W are the nearest-neighbor distance for sulfonate multiplets and water clusters, respectively. The parameter $\bar{R}$ is the correlation length for density-density fluctuations of sulfonates. The dimensionless parameters χ_S and χ_W are the number of head groups and number of water molecules in a multiplet, respectively.

Membrane η_1									
λ	R_A^S	R_B^S	$\bar{R}$	R_A^W	R_B^W	χ_S	χ_W	χ_W/χ_S	D (cm^2/sec)
0	1.86	3.36	3.5			16			
1	1.65	2.77	2.63	1.65	2.77	10	10	1	2.7×10^{-6}
3	1.72	2.84	2.7	1.72	2.84	10	30	3	4.5×10^{-6}
5	1.75	2.98	2.8	1.75	2.98	10	50	5	5.2×10^{-6}
0	1.75	3.29	3.49			22			
1	1.47	2.77	2.67	1.68	2.7	13	17	1.2	3.5×10^{-6}
3	1.54	2.8	2.8	1.79	2.81	13	62	4.5	5.2×10^{-6}
5	1.61	2.87	2.92	1.82	2.91	13	101	7.8	6.5×10^{-6}

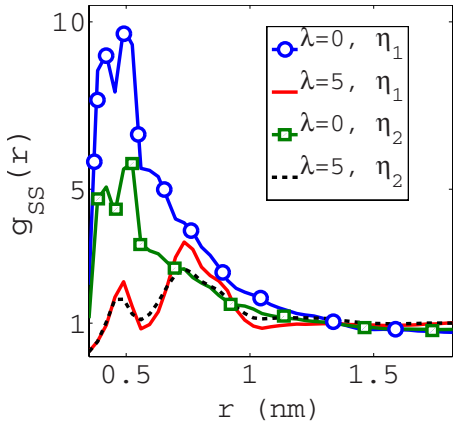

FIG. 5. (Color online) Sulfonate-sulfonate pair correlation function $g_{SS}(r)$ as a function of the sulfur-sulfur separation distance r. Membrane η_1: blue line with circles-Run 1, full red line-Run 4. Membrane η_2: green line with squares-Run 1, dashed black line-Run 4.

fonates is isotropic, and hence depends only on the modulus $q=|\vec{q}|$ of the wave vector. The calculated structure factors $S(q)$ for the dry and hydrated membranes are presented in Fig. 6. The ionomer-peak position in the low q-region corresponds to the length of the density-density correlations $\bar{R}=2\pi/q$ of sulfonates [17,40,54,55].

The nearest-neighbor distance between the multiplets can also be deduced, though less precisely, from the position of the long-range maximum R_B^S of the pair correlation functions $g_{SS}(r)$ in Fig. 4. As in the multiplet splitting effect, corresponding to the reduction in the multiplet size R_A^S at the onset of membrane solvation, the nearest-neighbor distance R_B^S also decreases to smaller values according to the results of Run 1 and Run 2. This is a consequence of the increase in the multiplet population $\xi=N_S/\chi_S$. For example, the number of multiplets in the membrane η_1 increases from $\xi=30$ in the dry membrane to $\xi=50$ in the hydrated membrane. The calculated values for $\bar{R}$ and R_B^S, seen in Table II, match each

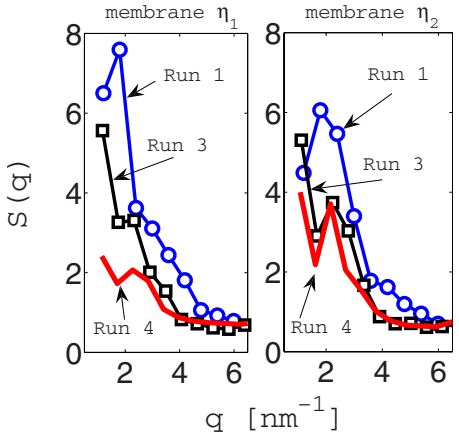

FIG. 6. (Color online) Small angle ionomer-peak region of sulfonate-sulfonate structure factor $S(q)$ for the membranes η_1 and η_2. Line with blue circles-Run 1, line with black squares-Run 3, full red line-Run 4. The step size $\delta q=2\pi/L\approx 0.5$ nm^{-1} defines the resolution along the x axis.

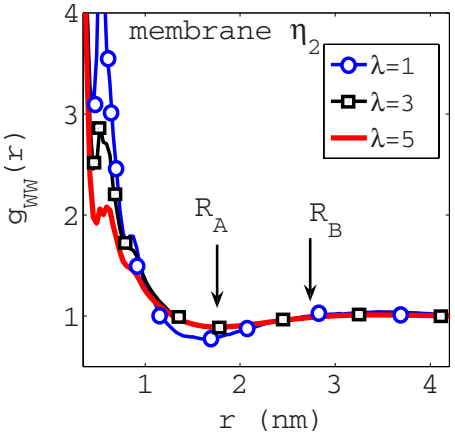

FIG. 7. (Color online) Water-water pair correlation function $g_{WW}(r)$ for the membrane η_2 as a function of the water-water separation distance r for Runs 2–4 from Table I. Line with blue circles—Run 2, line with black squares-Run 3, full red line-Run 4. The arrows show the average multiplets size R_A^W and the separation distance R_B^W between the water clusters. The calculated values for the parameters R_A^W and R_B^W are given in Table II.

other perfectly. We note that the increase of the average multiplet separation distance $\bar{R}$ for Runs 2–4 is a clear sign of membrane swelling, which is in accord with the results of Refs. [3,40,50].

C. Swollen multiplets inside a water shell

The pair correlation and the structure factor analysis, implemented in the previous subsection, can be also exploited to examine the water clustering features in hydrated membranes for Runs 2–4. We calculate the size of the water cluster R_A^W from the water-water correlation $g_{WW}(r)$ shown in Fig. 7. The nearest-neighbor cluster separation distances R_B^W were evaluated from the water-water structure factors. The calculated values for both parameters are given in Table II. There is good agreement between the water-water and the sulfonate-sulfonate multiplet nearest-neighbor distances R_B^W and R_B^S. This is an indirect verification of the fact that the ionomer cluster is a mixture of sulfonates and absorbed water molecules. The distribution of water molecules inside the ionomer cluster can be analyzed by comparing the water cluster size R_A^W with the sulfonate multiplet size R_A^S. Whereas for the membrane η_1 there is an excellent match between these two parameters, for the membrane η_2 the water clusters are consistently bigger than the sulfonate multiplets. Based on this result we conclude that a part of the total water loading per multiplet in fact exists outside the multiplet boundaries. This "outer" water shell encapsulates the multiplet and facilitates the formation of narrow water channels between the swollen multiplets. These channels, clearly seen in Fig. 3, are the pathways through which the ionomer absorbs more solvent upon its hydration. The water channels are also an attractive place for the unclustered head groups, and assist the ion diffusion between neighboring multiplets. We remark that free bulklike water would form in the interior of the multiplet only at sufficiently high solvation levels λ [56], a case not considered in this work.

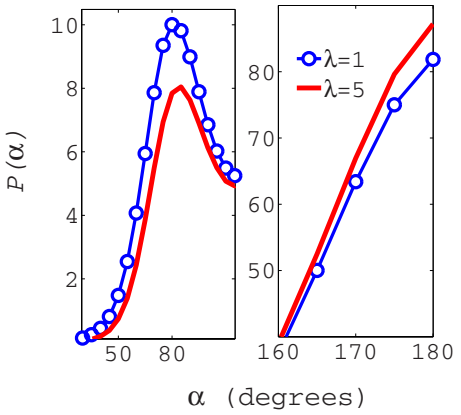

FIG. 8. (Color online) The probability distribution $P(\alpha)$ of the dihedral angle along the side chain of membrane η_1. Line with blue circles-Run 2, full red line-Run 4. The areas of the *gauche* conformation (α=82°) and the *trans* conformation (α=180°) are shown separately.

The average number of water molecules χ_W per water cluster was calculated by using Eq. (9) for $g_{WW}(r)$. This parameter, together with the parameter describing the water-per-sulfonate ratio χ_W/χ_S are given in Table II. For the membrane η_1 we obtain $\chi_W/\chi_S=\lambda$, a predicted result for the ionomer cluster with $R_A^W=R_A^S$. However for the membrane η_2 the ratio $\xi_W/\xi_S>\lambda$. This unexpected result can be interpreted in the following manner: when the sulfonate concentration approaches the percolation threshold for head groups, a fraction of the sulfonates are randomly distributed between the existing multiplets. These bridging sulfonates cannot retain their full solvation shell with λ water molecules in the hostile environment of hydrophobic backbones. The excess water molecules stripped from these "bulk" sulfonates are consequently redistributed between the existing multiplets. This leads to the formation of an outer solvent shell around each multiplet.

D. Swelling-induced ionomer deformation

The polymer backbone and side chains sustain conformational changes when the membrane swells. Two different types of deformation, an elongation (stretching) deformation and a coiling (frustration) deformation of polymer chains can

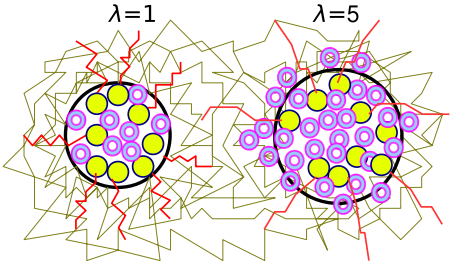

FIG. 9. (Color online) Schematics explaining the side-chain stretchinglike relaxation as a result of multiplet swelling from λ=1 to λ=5. The small hollow spheres are the water molecules, gray (yellow in online version) small spheres with attached tails are for side chains, big spheres represent the multiplets.

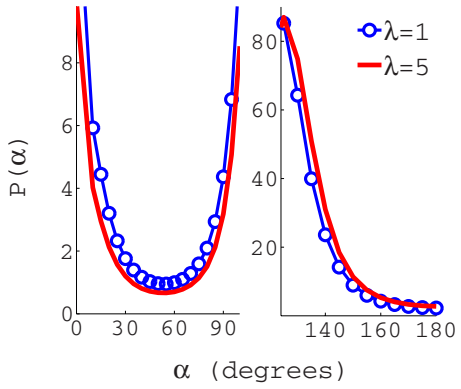

FIG. 10. (Color online) The probability distribution $P(\alpha)$ of the dihedral angle along the backbone of membrane η_1. Line with blue circles-Run 2, full red line-Run 4. The areas of a *cis* conformation (α=0°) and the *gauche* conformation (α=125°) are shown separately.

be conveniently resolved using the probability distribution $P(\alpha)$ of the dihedral angle along the polymer chains.

The probability distribution $P(\alpha)$ of the dihedral angle along the side chain is shown in Fig. 8 for the membrane η_1. The side chains have two *gauche* (±82°) and one *trans* conformations. When the membrane absorbs water, the side chains undergo a deformation in which a part of the *gauche* conformations transform into *trans* conformations. The overall effect of this structural deformation is a structural relaxation of the side chains, perceived as a stretching—an impact schematically illustrated in Fig. 9. We have also detected a similar stretchinglike structural relaxation for the backbone segments. As seen from Fig. 10, the probabilities of the two *gauche* (±125°) and single *cis* (±0°) backbone conformations in the solvated membrane diminish when the hydration parameter λ decreases.

The extent of side-chain relaxation sensitively depends on the sulfonate concentration η. In Fig. 11 we compare the $P(\alpha)$ curves for the two membranes. It is noticeable that the side chains are in a more relaxed state in the membrane η_1

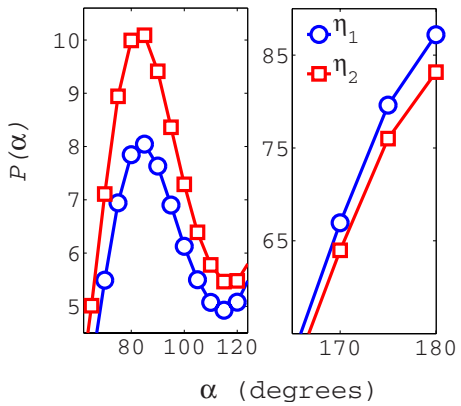

FIG. 11. (Color online) The probability distribution $P(\alpha)$ of the dihedral angle along the side chains. Line with blue circles-membrane η_1, line with red squares-membrane η_2. The areas of the *gauche* conformation (α=82°) and the *trans* conformation (α=180°) are shown separately.

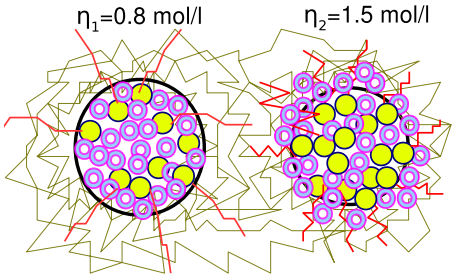

FIG. 12. (Color online) Schematic pictures explaining the differences between the stretchinglike relaxation of side chains for the membranes η_1 and η_2. The small hollow spheres are the water molecules, gray (yellow in online version) small spheres with attached tails are for side chains, big spheres represent the multiplets.

compared to the membrane η_2. This is a direct consequence of the fact that the smaller number of head groups inside the multiplet provide a more relaxed configuration for side chains compared to the case when a larger number of sulfonates are immersed into a smaller multiplet. The dihedral frustration of side chains in the high-sulfonate membrane is schematically illustrated in Fig. 12. A similar dihedral frustration has also been detected for the backbone polymer: in the high-sulfonate membrane the backbone segments adopt a more curly conformation.

E. Ion diffusion

The ion mobility in solvated ionomers is strongly affected by ion-head group association effects. On the one hand, this association localizes the ions near the head groups, and therefore decreases the rate of vehicular diffusion across the membrane. On the other hand, the localization effect increases the rate of the hopping diffusion of ions from sulfonate to sulfonate. This so-called surface diffusion is believed to be additionally enhanced by the water-ion electrostatic interactions and the side-chain thermal fluctuations. The strength of the ion-sulfonate association is commonly evaluated in the terms of the ion distribution around the head groups. Our simulation results for the sulfur-ion pair correlation function $g_{SH}(r)$ are plotted in Fig. 13. The first ion shell, seen as a very high peak on the left side of Fig. 13, originates from the attractive Coulomb forces between the ions and the SO_3^- groups. The second peak of $g_{SH}(r)$ on the right side of Fig. 13 arises from the ion shells of neighboring sulfonates in the multiplet. The condensation effect of ions on the sulfonates is noticeably stronger in the membrane η_1 than in the case of the membrane η_2. As a consequence, the ion mobility in the membrane η_2 will be higher.

The effect of a ion-sulfonate association also depends on the membrane hydration level λ [51]: the association is weak for the hydrated membrane with λ=1, whereas it is strong for the membrane with λ=5. The position of the minimum of $g_{SH}(r)$ corresponds to the position of the first maximum of $g_{SS}(r)$ in Fig. 4.

The mean square displacements (msd) of ions for different membrane hydrations λ are plotted in Fig. 14. As is expected from the ion delocalization effect in hydrated membranes, higher membrane hydrations result in larger ion

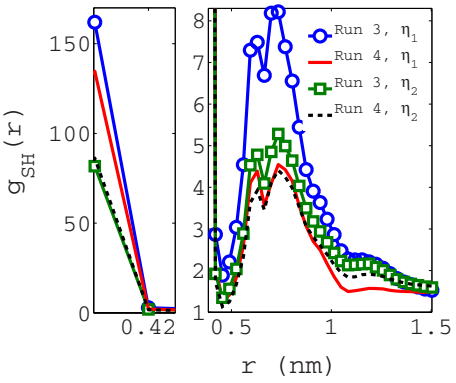

FIG. 13. (Color online) Sulfonate-ion correlation function $g_{SH}(r)$ as a function of the separation distance r. The first and second peak areas are shown separately. Membrane η_1: blue line with circles-Run 3, full red line-Run 4. Membrane η_2: green line with squares-Run 3, dashed black line-Run 4.

displacements [50]. The msd result for the membrane η_1 is below the corresponding result for the membrane η_2 for Run 4. This happens partly due to the strong ion delocalization effect, and partly due to the small nearest-neighbor distances R_B^S in the membrane η_2.

The calculated values for the diffusion coefficient of ions,

$$D = \lim_{t\to\infty} \frac{\mathrm{msd}(t)}{6t}, \tag{11}$$

are gathered in Table II. The ion diffusion, similar to the ion mobility, is stronger in membrane η_2 than in membrane η_1 because of the low ion-sulfonate association. There are two other factors that contribute to the ion diffusion of membrane η_2: the existence of "bulk" sulfonates between neighboring multiplets and the accumulation of water molecules around the multiplets. Both these factors can lead to the formation of temporary bridges, sulfonic and/or solvent in nature, between the multiplets. Our results for ion diffusion are in good agreement with the simulation results of Ref. [50]. However they are small compared to the ion diffusion coefficients ex-

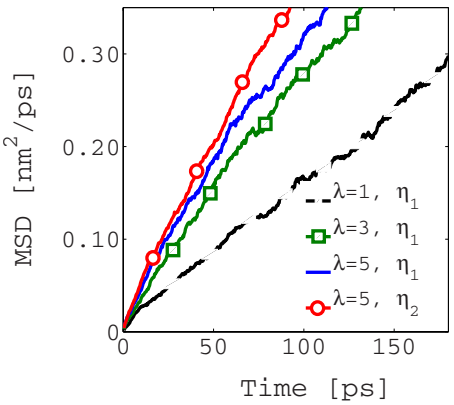

FIG. 14. (Color online) Mean squared displacement of ions as a function of time for Runs 2–4. Membrane η_1: dashed black line-Run 2, green line with squares-Run 3, full blue line-Run 4. Membrane η_2: red line with circles-Run 4.

perimentally observed in fully hydrated Nafion ionomers. This discrepancy is most probably not due to our neglect of the Grotthuss mechanism, which is strongly suppressed when λ is small [57–59], but is a consequence of the reduced number of pathways in our low-humidity, low-sulfonate model.

V. DISCUSSION

We have investigated the swelling properties of multiplets in low humidity ionomers with low sulfonate concentration by examining different models for the side-chain architecture. Our primary goal was to determine the dependence of multiplet swelling on the hydration level λ and the sulfonate concentration η of the membrane.

Our main result is the fission of the sulfonate multiplets into smaller parts at the onset of membrane hydration. This behavior is not explained by the classical theories of cluster swelling in ionomers, according to which the swelling should be a continuous and monotonic process of multiplet expansion. We hypothesize that both the additional screening brought into the membrane by adsorbed water, and the solvation of sulfonates by water molecules contribute to the multiplet fission. For hydrated multiplets the fission is replaced by swelling when λ is further increased. The resultant small multiplets will consequently swell, keeping the number of their sulfonate population constant, when more water is absorbed into the membrane. We have also found that the location of water in low-sulfonate membranes strongly depends on the sulfonate concentration. For a relatively low sulfonate concentration nearly all sulfonate groups are in multiplet formations. The average water loading parameter per multiplet χ_W/χ_S, where χ_W is the number of water molecules belonging to the multiplet, and χ_S is the number of sulfonates in the multiplet, perfectly matches the water content of the membrane λ. However, for relatively high sulfonate concentrations, the water loading parameter per multiplet χ_W/χ_S is consistently larger than the parameter λ for the membrane hydration levels considered. We assume that, when the sulfonate concentration approaches the percolation threshold for head groups, a fraction of the sulfonates are randomly distributed between the existing multiplets. These bridging sulfonates cannot retain their full solvation shell in the hostile environment of hydrophobic backbones. The excess water molecules stripped from these bulk sulfonates are consequently redistributed between the existing multiplets. The results of our structural analysis confirm the formation of unexpected water shells around sulfonate multiplets. The multiplet fission and the water encapsulation effects are illustrated schematically in Fig. 15.

Our discovery of the uneven distribution of the water-to-sulfonate loading in the ionomer opens a new window into the percolation characteristics of the hydrophilic network in ionomers. It is no longer sufficient to have a continuous pathway among sulfonates in order for percolation of ions to occur, as some of these sulfonates may be found in the hydrophobic material, where they are not capable of contributing to ion transport. The predicted hydration levels necessary for good transport of ions will thus be higher than they would be if the presence of sulfonates encapsulated in backbone material were ignored.

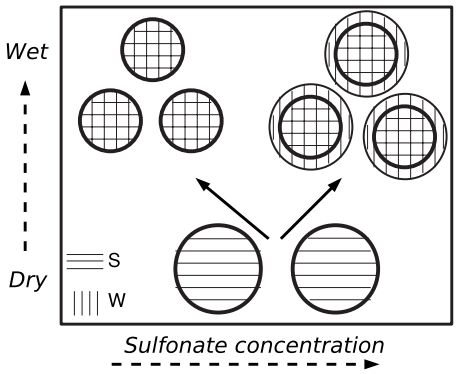

FIG. 15. Schematic illustration of the multiplet hydration. At a low sulfonate concentration the hydrated multiplets consist of sulfonates and water molecules. At a higher sulfonate concentration each of the multiplets is surrounded by a water shell. The splitting of dry multiplets into smaller hydrated multiplets is also sketched. Vertical/horizontal hatching is used for the water (W) and the sulfonate (S) areas of the multiplet.

We have also analyzed the structural deformations occurring in the ionomer as a result of membrane swelling, and found that in swollen membranes the ionomer is in a more relaxed state. The degree of relaxation, however, is sensitive to the sulfonate concentration: the side chains and backbones are found to be more relaxed in low-sulfonate membranes. This result is a direct consequence of the fact that in low-sulfonate membranes the sulfonate cluster is less dense, and can relax more readily than in the denser environment of the high-sulfonate material. However, ion diffusion is stronger in high-sulfonate membranes, and can potentially benefit from the formation of temporary solvent and sulfonate bridges between the multiplets.

An interesting question, yet to be resolved, is whether the multiplet splitting and shrinking effects depend on the pretreatment history of the membrane. The membrane morphology is known to be affected by the type of pretreatment, such as boiling, annealing, drying, poling, stretching, etc., and by the order in which these steps are taken. In most cases the impact of the pretreatment is either the formation of a new morphology with an anisotropy in the backbone and side-chain orientations, or the reshaping of the network of hydrophilic clusters. In our current work the dry membrane was "numerically pretreated" by our fragmentation and defragmentation procedures, as described in Sec. III. We assume that our membrane has a network of hydrophilic pores resembling the network in a mold-extruded membrane, provided it has then been annealed.

In order to analyze the consequences of the residual anisotropy in the ionomer on the multiplet reorganization effects reported in this work, we carried out test simulations for a poled and dry Nafion-like ionomer. According to our previous results on ionomer poling [33], rodlike aggregations of head groups are formed along the direction of the applied electric field. The poled structures were found to be stable after the release of the poling field. One of the poled structures of Ref. [33] was used as a starting configuration for

Run 1 of our current work. Our simulation result indicated that a similar reorganization effect of sulfonate multiplets, as seen in the case of isotropic membranes, takes place. Hence, we conclude that the splitting and shrinking effects are robust against structural anisotropy in the membrane.

We also performed test simulations to clarify the nature of multiplet reorganization in dry membranes that had been previously swollen. The hydrated membrane from Run 4 with water content $\lambda=5$ was first dried through a simple elimination of all water molecules in the simulation box. Then the water-free membrane was gradually shrunk to the system size used for Run 1. The results obtained show that the initially dry membrane, membrane I, and the pretreated dry membrane, membrane II, have different structures. In the latter the multiplet sizes R_A^S were smaller and close to the multiplet sizes corresponding to Run 2. However, after annealing at high temperatures, the discrepancies between the membranes disappeared, and both membranes exhibited the splitting and shrinking of multiplets at the onset of hydration.

In future work, we plan to extend the model presented here to take into account the partial charges on the side-chain monomers. Our preliminary results indicate that a partial delocalization of the negative charge along the side-chain head group has a noticeable role in the membrane swelling process.

ACKNOWLEDGMENTS

We thank E. Spohr and R. Wycisk for valuable comments during the preparation of this paper. This work was supported by the US Department of Energy under grant DE-FG02-05ER46244 and by the German Science Foundation (DFG) under Grant No. SFB TR6 (D1). It was made possible by use of facilities at the Case ITS High Performance Computing Cluster and the Ohio Supercomputing Center.

[1] A. McAlevy, U.S. Patent No. 2,405,971 (29 August 1946).
[2] M. I. Perry and T. F. Fuller, J. Electrochem. Soc. **149**, S59 (2002).
[3] A. Sacca, A. Carbone, R. Pedicini, G. Portale, L. D'Ilaro, A. Longo, A. Martorana, and E. Passalacqua, J. Membr. Sci. **278**, 105 (2006).
[4] M. Saito, K. Hayamizu, and T. Okada, Phys. Chem. B **109**, 3112 (2005).
[5] K. D. Kreuer, J. Membr. Sci. **185**, 29 (2001).
[6] B. Smitha, S. Sridnar, and A. A. Khan, J. Polym. Sci., Part B: Polym. Phys. **43**, 1538 (2005).
[7] D. J. Connolly and W. F. Gresham, U.S. Patent No. 3,282,875 (1 November 1966); D. A. Hounshell and J. K. Smith, Jr., *Science and Corporate Strategy: DuPont R&D, 1902-1980* (Cambridge University Press, Cambridge, England, 1988).
[8] S. Banerjee and D. E. Curtin, J. Fluorine Chem. **125**, 1211 (2004).
[9] W. Y. Hsu and T. D. Gierke, Macromolecules **15**, 101 (1982); J. Membr. Sci. **13**, 307 (1983); T. D. Gierke, G. E. Munn, and F. C. Wilson, J. Polym. Sci. Phys. Ed. **19**, 1687 (1981).
[10] M. A. F. Robertson, Ph.D. thesis, University of Calgary, 1994.
[11] N. H. Jalani, Ph.D. thesis, Worcester Polytechnic Institute, 2006.
[12] K. A. Mauritz, C. J. Hora, and A. J. Hopfinger, Polym. Prepr. (Am. Chem. Soc. Div. Polym. Chem.) **19**, 324 (1978); K. A. Mauritz and C. E. Rogers, Macromolecules **18**, 483 (1985).
[13] K. A. Mauritz and R. B. Moore, Chem. Rev. **104**, 4535 (2004).
[14] H. L. Yeager and A. Steck, J. Electrochem. Soc. **128**, 1880 (1981).
[15] A. Eisenberg, Macromolecules **3**, 147 (1970); **30**, 7914 (1997).
[16] M. H. Litt, Polym. Prepr. (Am. Chem. Soc. Div. Polym. Chem.) **38**, 80 (1997).
[17] G. Gebel and O. Diat, Fuel Cells **5**, 261 (2005); L. Rubatat, O. Diat, and G. Gebel,Macromolecules **37**, 7772 (2004).
[18] K. Schmidt-Rohr and Q. Chen, Nature Mater. **7**, 75 (2008).
[19] S. J. Paddison, D. W. Reagor, and T. A. J. Zawodzinski, J. Electroanal. Chem. **91**, 459 (1998).
[20] S. Slade, S. A. Campbell, T. R. Ralph, and F. C. Walsh, J. Electrochem. Soc. **149**, A1556 (2002).
[21] M. Cappadonia, J. W. Erning, and U. Stimming, J. Electroanal. Chem. **376**, 189 (1994).
[22] H.-L. Lin, T. L. Yu, and F.-H. Han, J. Polym. Res. **13**, 379 (2006).
[23] H.-L. Lin, T. L. Yu, C.-H. Huang, and T.-L. Lin, J. Polym. Sci., Part B: Polym. Phys. **43**, 3044 (2005).
[24] V. Arcella, C. Trogila, and A. Ghielmi, Ind. Eng. Chem. Res. **44**, 7646 (2005).
[25] Y. Yamamoto, M. C. Ferrari, M. Giacinti, M. G. Baschetti, M. G. De Angelis, and G. C. Sarti, Desalination **200**, 636 (2006).
[26] J. Fimrite, H. Struchtrup, and N. Djilali, J. Electrochem. Soc. **152**, A1804 (2005).
[27] M. Laporta, M. Pegoraro, and L. Zanderighi, Phys. Chem. Chem. Phys. **1**, 4619 (1999).
[28] S. Lue and S. J. Shieh, J. Macromol. Sci., Phys. **48**, 114 (2009).
[29] S. Dokmaisrijan and E. Spohr, J. Mol. Liq. **129**, 92 (2006).
[30] J. T. Wescott, Y. Qi, L. Subramanian, and T. W. Capehart, J. Chem. Phys. **124**, 134702 (2006).
[31] D Wu, S. J. Paddison, and J. A. Elliott, Macromolecules **42**, 3358 (2009).
[32] E. Allahyarov and P. Taylor, J. Chem. Phys. **127**, 154901 (2007).
[33] E. Allahyarov and P. L. Taylor, Phys. Rev. E **80**, 020801(R) (2009).
[34] A. Vishnyakov and A. V. Neimark, J. Phys. Chem. B **105**, 7830 (2001); **105**, 9586 (2001).
[35] E. Allahyarov and P. Taylor, J. Phys. Chem. B **113**, 610 (2009).
[36] Z. Lu, G. Polizos, D. D. Macdonald, and E. Manias, J. Electrochem. Soc. **155**, B163 (2008).
[37] C. G. Vayenas, M. N. Tsampas, and A. Katsaounis, Electrochim. Acta **52**, 2244 (2007).
[38] S. J. Paddison and T. A. Zawodzinski, Solid State Ion. **113-**

115, 333 (1998).
[39] S. J. Paddison, Annu. Rev. Mater. Res. **33**, 289 (2003).
[40] G. Gebel and R. B. Moore, Macromolecules **33**, 4850 (2000).
[41] S. J. Paddison and J. A. Elliott, J. Phys. Chem. **109**, 7583 (2005).
[42] R. Jinnouchi and K. Okazaki, J. Electrochem. Soc. **150**, E66 (2003).
[43] J. A. Elliott, S. Hanna, A. M. S. Elliott, and G. E. Cooley, Phys. Chem. Chem. Phys. **1**, 4855 (1999).
[44] S. S. Jang, V. Molinero, T. Cagin, and W. A. Goddard III, J. Phys. Chem. B **108**, 3149 (2004).
[45] K. Chan, Y. W. Tang, and I. Szalai, Mol. Simul. **30**, 81 (2004).
[46] A temporary fragmentation of ionomer molecules into smaller segments in order to speed up its equilibration in molecular dynamics simulations is equivalent of heating up the ionomer above its glass transition temperature T_g in experiments.
[47] A. Vishnyakov and A. V. Neimark, J. Phys. Chem. B **104**, 4471 (2000).
[48] D. Rivin, G. Meermeier, N. S. Schneider, A. Vishnyakov, and A. V. Neimark, J. Phys. Chem. B **108**, 8900 (2004).
[49] M. Mazars, J. Chem. Phys. **115**, 2955 (2001).
[50] S. Cui, J. Liu, M. E. Selvan, D. J. Keffer, B. J. Edwards, and W. V. Steele, J. Phys. Chem. B **111**, 2208 (2007).
[51] S. Cui, J. Liu, M. E. Selvan, S. J. Paddison, D. J. Keffer, and B. J. Edwards, J. Phys. Chem. B **112**, 13273 (2008).
[52] G. Brunello, S. G. Lee, S. S. Jang, and Y. Qi, J. Renewable Sustainable Energy **1**, 033101 (2009).
[53] E. Spohr, Mol. Simul. **30**, 107 (2004).
[54] J. A. Elliott, S. Hanna, A. M. S. Elliott, and G. E. Cooley, Polym. Eng. Sci. **46**, 228 (2006).
[55] S. K. Young, S. F. Trevino, and N. C. Tan, J. Polym. Sci., Part B: Polym. Phys. **40**, 387 (2002).
[56] P. Choi, N. H. Jalani, and R. Datta, J. Electrochem. Soc. **152**, E123 (2005).
[57] D. Seeliger, C. Hartnig, and E. Spohr, Electrochim. Acta **50**, 4234 (2005).
[58] M. Eikerling, A. A. Kornyshev, and U. Stimming, J. Phys. Chem. **101**, 10807 (1997).
[59] E. L. Thompson, T. W. Capehart, T. J. Fuller, and J. Jorne, J. Electrochem. Soc. **153**, A2351 (2006).
[60] G. Dorenbos and Y. Suga, J. Membr. Sci. **330**, 5 (2009).